



OPEN

## Relationship between ion currents and membrane capacitance in canine ventricular myocytes

Balázs Horváth<sup>1,2</sup>✉, Zsigmond Kovács<sup>1</sup>, Csaba Dienes<sup>1</sup>, Zalán Barta<sup>1</sup>, József Óvári<sup>1</sup>, Norbert Szentandrassy<sup>1,3</sup>, János Magyar<sup>1,4</sup>, Tamás Bányász<sup>1,6</sup> & Péter P. Nánási<sup>1,5,6</sup>

Current density, the membrane current value divided by membrane capacitance ( $C_m$ ), is widely used in cellular electrophysiology. Comparing current densities obtained in different cell populations assume that  $C_m$  and ion current magnitudes are linearly related, however data is scarce about this in cardiomyocytes. Therefore, we statistically analyzed the distributions, and the relationship between parameters of canine cardiac ion currents and  $C_m$ , and tested if dividing original parameters with  $C_m$  had any effect. Under conventional voltage clamp conditions, correlations were high for  $I_{K1}$ , moderate for  $I_{Kr}$  and  $I_{Ca,L}$  while negligible for  $I_{Ks}$ . Correlation between  $I_{to1}$  peak amplitude and  $C_m$  was negligible when analyzing all cells together, however, the analysis showed high correlations when cells of subepicardial, subendocardial or midmyocardial origin were analyzed separately. In action potential voltage clamp experiments  $I_{K1}$ ,  $I_{Kr}$  and  $I_{Ca,L}$  parameters showed high correlations with  $C_m$ . For  $I_{NCX}$ ,  $I_{Na,late}$  and  $I_{Ks}$  there were low-to-moderate correlations between  $C_m$  and these current parameters. Dividing the original current parameters with  $C_m$  reduced both the coefficient of variation, and the deviation from normal distribution. The level of correlation between ion currents and  $C_m$  varies depending on the ion current studied. This must be considered when evaluating ion current densities in cardiac cells.

**Keywords** Cardiac ion currents, Membrane capacitance, Current densities, Current integrals, Dog myocytes, Action potential voltage clamp

### Abbreviations

$C_m$	Membrane capacitance
CVC	Conventional voltage clamp
APVC	Action potential voltage clamp
CV	Coefficient of variation
$I_{K(ACh)}$	Acetylcholine-sensitive potassium current
$I_{Ca,L}$	L-type $Ca^{2+}$ current
$I_{NCX}$	$Na^+/Ca^{2+}$ exchanger current
$I_{Na,late}$	Late $Na^+$ current
$I_{Kr}$	Rapid delayed rectifier $K^+$ current
$I_{Ks}$	Slow delayed rectifier $K^+$ current
$I_{K1}$	Inward rectifier $K^+$ current
$I_{to1}$	Transient outward $K^+$ current
$Q_x$	The charge carried by ion current “x” ( $I_x$ integral)
r	Pearson's correlation coefficient
$\rho$	Spearman's correlation coefficient
$\phi$	Effect size
EPI	Subepicardial cells
ENDO	Subendocardial cells
MID	Mid-myocardial cells

<sup>1</sup>Department of Physiology, Faculty of Medicine, University of Debrecen, Debrecen, Hungary. <sup>2</sup>Faculty of Pharmacy, University of Debrecen, Debrecen, Hungary. <sup>3</sup>Department of Basic Medical Sciences, Faculty of Dentistry, University of Debrecen, Debrecen, Hungary. <sup>4</sup>Division of Sport Physiology, Department of Physiology, Faculty of Medicine, University of Debrecen, Debrecen, Hungary. <sup>5</sup>Department of Dental Physiology and Pharmacology, Faculty of Dentistry, University of Debrecen, Debrecen, Hungary. <sup>6</sup>These authors contributed equally: Tamás Bányász and Péter P. Nánási. ✉email: horvath.balazs@med.unideb.hu

Ion current density is the membrane current value divided by the measured cell membrane capacitance ( $C_m$ ). This process is usually referred to as “normalizing” current values to the obtained  $C_m$ , which serves as the consensual surrogate measure for the cell surface area. In scientific publications about cellular electrophysiology, ion current magnitudes obtained on different cell populations are expected to be reported and compared based on their ion current densities. This convention assumes linear relationships between magnitudes of ion currents,  $C_m$ , and the cell surface area. In simple terms, bigger cells are expected to generate larger currents. It is widely believed that using current densities instead of absolute current amplitudes decreases the variability of experimental results, and therefore might help in demonstrating real biological differences with statistical methods.

Transmembrane currents,  $C_m$  and cell surface area are linearly related to each other if (1) the cell membrane composition and (2) the ion channel distribution in the cell membrane is homogeneous, and if (3)  $C_m$  can be measured accurately. This concept seems to be trivial in small spheroid cells such as red and white blood cells<sup>1,2</sup>, or cells with non-articulated cell surface membrane like neuronal axons<sup>3</sup>. These assumptions, however, are not as intuitive in cardiomyocytes, which are large cells having highly articulated and compartmentalized cell surface membrane with intercalated discs and extensive axial- and transversal tubular network. In fact, the actual relations between transmembrane current,  $C_m$  and cell surface area in cardiac muscle cells are largely unknown.

Recently, Ismaili et al. studied the relationship between  $C_m$  and L-type calcium current ( $I_{Ca,L}$ ) amplitude in human and rodent atrial and ventricular cardiomyocytes<sup>4</sup>, while Kula and coworkers performed similar studies with inward rectifier potassium current ( $I_{K1}$ ), acetylcholine-sensitive potassium current ( $I_{K(ACH)}$ ), and transient outward potassium current ( $I_{to}$ ) in rat ventricular cells<sup>5,6</sup>. All these studies reported significant deviations from normal data distribution together with sometimes surprisingly low correlations between current amplitudes and  $C_m$ , with  $r^2$  ranging from 0.17 to 0.28 in<sup>4</sup>, and  $r$  values being 0.04 for  $I_{to}$ , 0.42 for the constitutively active-, and 0.61 for the acetylcholine-induced component of  $I_{K(ACH)}$ , while 0.84 for  $I_{K1}$ <sup>6</sup>.

Computational models and experimental studies indicate that large variations between individual cells exist in ion channel activity that may underlie electrophysiological heterogeneity within the human population<sup>7,8</sup>. Similarly, Ballouz et al. showed large variation in mRNA levels for a wide range of cardiac proteins involved in regulating cellular electrophysiological properties<sup>9</sup>, whereas Lachaud et al. have shown significant inter-cell variability in ventricular APD<sup>10</sup>. Despite these substantial variations in electrophysiological characteristics, bioelectricity of the heart can most likely be properly coordinated because of overlapping functions and certain well-defined correlations between ion currents<sup>11,12</sup>. Most recently, similar relationships in mRNA transcript levels<sup>9</sup> and in cardiac ion channel co-translation<sup>13</sup> have also been shown.

In this study, we systematically investigated the relationship between  $C_m$  and the major cardiac ion currents (L-type calcium current— $I_{Ca,L}$ ; late sodium current— $I_{Na,late}$ ; sodium-calcium exchange current— $I_{NCX}$ ; inward rectifier potassium current— $I_{K1}$ ; rapid delayed rectifier potassium current— $I_{Kr}$ ; slow delayed rectifier potassium current— $I_{Ks}$ ) in canine ventricular myocytes under conventional voltage clamp (CVC) as well as action potential voltage clamp (APVC) conditions. Dogs were chosen because the electrophysiological properties of canine ventricular cells are known to be similar to those of human myocytes<sup>14–16</sup>. Besides investigating a broad range of ion currents, obtained under two different voltage clamp conditions, the novelties of the present study are the comprehensive statistical analyses of (1) the distribution of  $C_m$  and the ion current parameter values; (2) the relationship between  $C_m$  and the ion current parameters; and (3) the effect of “normalizing” the original membrane current parameters to  $C_m$ .

We have found generally good correlations between  $C_m$  and current amplitudes or integrals in this preparation, although correlations were occasionally limited by regional heterogeneity of ion channels and non-ideal experimental conditions.

## Results

### Membrane capacitance

The pooled membrane capacitance ( $C_m$ ) values of all cells involved in the study ( $n = 639$ ) significantly deviated from normal distribution ( $p < 0.001$ ; Supplementary Fig. 1). The distribution was right-skewed (skewness = 0.533) and leptokurtic (excess kurtosis = 0.561). The arithmetic mean of  $C_m$  was  $139.87 \pm 1.45$  pF, and median value was 139 pF. The observed effect size of the deviation from normal distribution was “small” ( $\phi = 0.228$ ), indicating that the magnitude of the difference between the sample distribution and the normal distribution was small.  $C_m$  values in any current groups did not deviate significantly from normal distribution, except in  $I_{Ks}$  measurements ( $p = 0.013$ ;  $\phi = 0.33$ ; Supplementary Fig. 1J) and when all cells were pooled together in  $I_{to1}$  measurements ( $p = 0.036$ ;  $\phi = 0.248$ ; Supplementary Fig. 3A) under CVC experiments.

### L-type $Ca^{2+}$ current ( $I_{Ca,L}$ )

$I_{Ca,L}$  was studied under CVC conditions in 198 myocytes (Fig. 1A).  $I_{Ca,L}$  peak current values (Fig. 1C) showed a significantly non-normal distribution, being left-skewed (towards higher current values; skewness =  $-0.546$ ), with normal kurtosis. The absolute coefficient of variation (CV) of  $I_{Ca,L}$  peak was 0.485. The distribution of data still remained significantly non-normal after dividing peak  $I_{Ca,L}$  with  $C_m$ , although the CV significantly ( $p = 0.02$ ) reduced to 0.398 after this operation (Supplementary Table 1).

The correlation between the amplitude of  $I_{Ca,L}$  and  $C_m$  was moderate (Spearman's  $\rho = -0.603$ ). The estimated current density was  $-6.7 \pm 0.63$  pA/pF (Fig. 1C). The close to zero ( $-42 \pm 89$  pA) value of the  $y$  intercept supports the actual linear relationship between  $C_m$  and  $I_{Ca,L}$ .

Under APVC conditions  $I_{Ca,L}$  was dissected as a  $1 \mu\text{M}$  nisoldipine-sensitive current (Fig. 1B) in 15 cells. In contrast to CVC experiments, the distribution of either the  $I_{Ca,L}$  current parameters (peak current, mid-plateau current, current integral— $Q_{Ca,L}$ ) or their values divided with  $C_m$  did not differ significantly from normal distribution

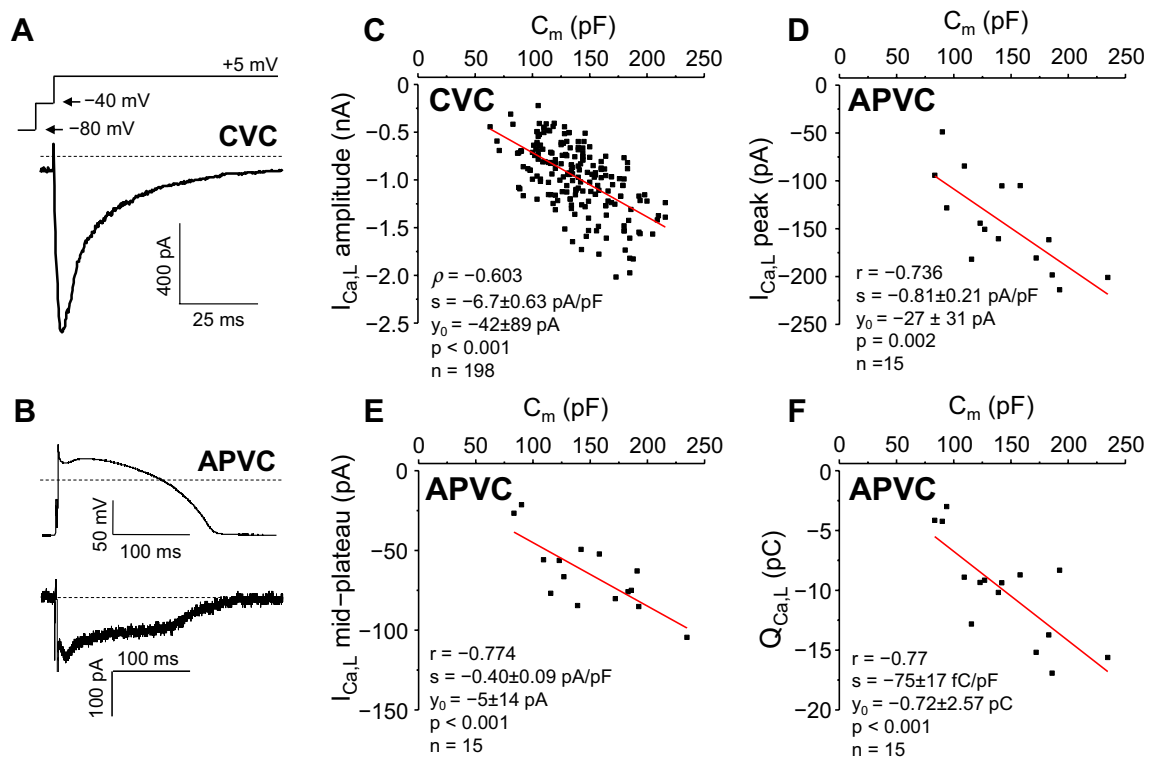


**Figure 1.** Correlation between  $C_m$  and  $I_{Ca,L}$  in canine ventricular myocytes. Left: representative  $I_{Ca,L}$  records obtained under CVC (A) and APVC (B) conditions, respectively. In both cases command signals are shown above the current records, dashed lines indicate zero voltage and current levels. Right: correlations between  $C_m$  and  $I_{Ca,L}$  peak amplitude measured at +5 mV under CVC conditions (C) and under APVC conditions (D), between  $C_m$  and mid-plateau  $I_{Ca,L}$  amplitude (E), and between  $C_m$  and  $I_{Ca,L}$  integral ( $Q_{Ca,L}$ ; F). Here and in all subsequent figures, red lines were obtained by simple linear regression, where  $r$  or  $\rho$  indicate the respective correlation coefficient,  $s$  is slope of the line (current density or charge density, given as mean  $\pm$  SEM),  $y_0$  is the intercept on  $y$  axis at  $C_m = 0$  pF,  $p$  is significance of slope, and  $n$  is the number of cells analyzed. CVC experiments: 198 cells from 77 animals; APVC experiments: 15 cells from 7 animals.

in any case, as determined in APVC experiments (Supplementary Table 2). CVs for these parameters all reduced upon dividing the original values with  $C_m$ , however, changes in CVs did not reach statistical significance.

Pearson's correlation coefficients were  $r = -0.74$  and  $r = -0.77$  for the peak and the mid-plateau values of  $I_{Ca,L}$ , as shown in Fig. 1D,E, respectively. Similarly, the charge carried by the current, indicated as  $Q_{Ca,L}$  ( $-75 \pm 17$  fC/pF) yielded a high correlation with  $C_m$  ( $r = -0.77$ ) (Fig. 1F). These values obtained for  $I_{Ca,L}$  density and  $Q_{Ca,L}$  are in a good agreement with earlier results obtained in canine ventricular myocytes<sup>16</sup>.

#### Late $Na^+$ current ( $I_{Na,late}$ )

$I_{Na,late}$  was recorded exclusively under APVC conditions as a 1  $\mu$ M GS-458967-sensitive current (Fig. 2A). Since its peak often did not separate from the decaying phase of  $I_{Na,early}$ , only mid-plateau amplitudes and current integrals ( $Q_{Na,late}$ ) were calculated and analyzed, as shown in Fig. 2B,C and in Supplementary Tables 3 and 6. Both the mid-plateau current values ( $p = 0.029$ ,  $\phi = 0.364$ ) and the total charge carried by the current ( $p = 0.037$ ,  $\phi = 0.392$ ) were significantly non-normally distributed, with medium  $\phi$  effect sizes, and CVs of 0.493 and 0.447, respectively. After dividing the original values with  $C_m$ , both distributions (mid-plateau  $I_{Na,late}/C_m$  and  $Q_{Na,late}/C_m$ ) became normal, with their CVs becoming non-significantly smaller (0.415 and 0.373, respectively).

Bivariate distributions of  $C_m$  and mid-plateau  $I_{Na,late}$  or  $C_m$  and  $Q_{Na,late}$  data pairs were not significantly different from the normal bivariate distribution. Pearson's correlation coefficients were  $r = -0.475$  for  $C_m$  and mid-plateau  $I_{Na,late}$ , and  $r = -0.483$  for  $C_m$  and  $Q_{Na,late}$ , respectively, indicating a low linear correlation of mid-plateau  $I_{Na,late}$  and  $Q_{Na,late}$  with  $C_m$ .

#### $Na^+/Ca^{2+}$ exchanger current ( $I_{NCX}$ )

$I_{NCX}$  was recorded exclusively under APVC conditions as a 0.5  $\mu$ M ORM-10962-sensitive current (Fig. 2D). Since its peak often did not separate well from the capacitive transient, we also present only mid-plateau current amplitudes and current integrals ( $Q_{NCX}$ ) here (Fig. 2E,F; Supplementary Tables 3 and 6).

Both original current values and current densities of mid-plateau  $I_{NCX}$  were normally distributed, with CVs of 0.403 for original values, and 0.348 for current densities, respectively.  $Q_{NCX}$  was significantly non-normally distributed with a large effect size ( $p = 0.024$ ,  $\phi = 0.613$ ), being left-skewed (towards higher current values;

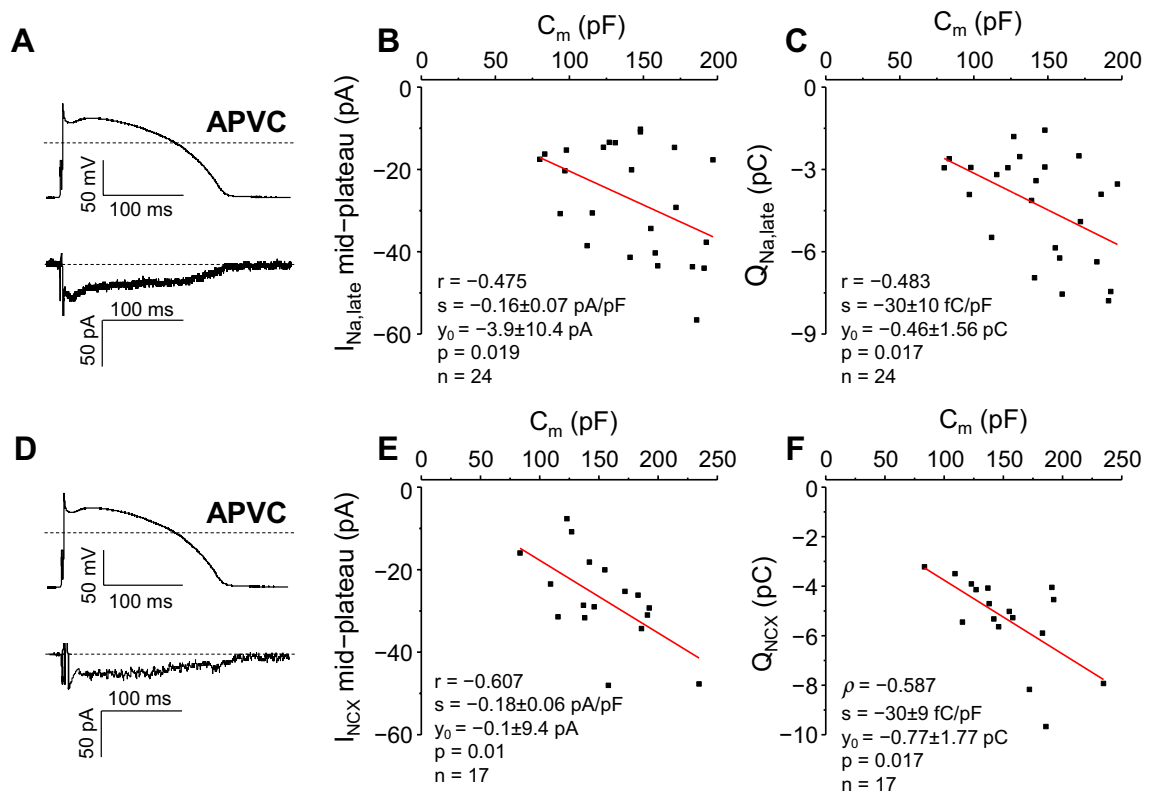


**Figure 2.** Correlation between  $C_m$  and  $I_{Na,late}$  (A–C), and between  $C_m$  and  $I_{NCX}$  (D–F). Left: representative  $I_{Na,late}$  (A) and  $I_{NCX}$  (D) records obtained under APVC conditions. Command action potentials are shown above the current traces, dashed lines indicate zero voltage and current levels. Right: B, E: correlations between  $C_m$  and mid-plateau currents; C, F: correlations between  $C_m$  and  $I_{Na,late}$  and  $I_{NCX}$  current integrals ( $Q_{Na,late}$ ,  $Q_{NCX}$ ).  $I_{Na,late}$  experiments: 24 cells from 10 animals,  $I_{NCX}$  experiments: 17 cells from 8 animals.

skewness =  $-1.274$ ). The distribution became normal after dividing  $Q_{NCX}$  with  $C_m$  ( $p = 0.172$ ), with CVs being 0.311 and 0.227, respectively.

Bivariate distribution of  $C_m$  and mid-plateau  $I_{NCX}$  data pairs was normal, whereas distribution of  $C_m$  and  $Q_{NCX}$  data pairs was significantly different from normal ( $p = 0.049$ ). Correlation coefficients were  $r = -0.607$  for  $C_m$  and mid-plateau  $I_{NCX}$ , and  $\rho = -0.587$  for  $C_m$  and  $Q_{NCX}$ , respectively, indicating moderate linear correlation between  $C_m$  and mid-plateau  $I_{NCX}$ , and moderate monotonic correlation between  $C_m$  and  $Q_{NCX}$ .

### Inward rectifier $K^+$ current ( $I_{K1}$ )

Both original  $I_{K1}$  peak (Fig. 3A) values and  $I_{K1}$  peak current densities showed normal distribution (with CVs being 0.309 and 0.246, respectively) under CVC conditions. The Forkman's test showed a significantly ( $p = 0.0495$ ) reduced CV after calculating  $I_{K1}$  peak current densities (Supplementary Table 1).

Bivariate distributions of  $C_m$  and  $I_{K1}$  peak amplitude data pairs were normal. These parameters highly correlated with each other ( $r = -0.72$ , Fig. 3C, Supplementary Table 4). Linear regression analysis yielded a slope of  $-57.5 \pm 5.9$  pA/pF.

Under APVC conditions  $I_{K1}$  was defined as a  $50 \mu\text{M}$   $\text{BaCl}_2$ -sensitive current (Fig. 3B) in 19 myocytes.  $I_{K1}$  current peaks as well as charges carried by  $I_{K1}$  ( $Q_{K1}$ ) were normally distributed in all cases of original values and after dividing them with  $C_m$ . CVs were 0.27 for  $I_{K1}$  peak current and 0.162 for  $I_{K1}$  peak current density, and 0.276 for  $Q_{K1}$  and 0.162 for  $Q_{K1}/C_m$ , respectively. Dividing original current parameters with  $C_m$  significantly reduced data variability in case of  $I_{K1}$  ( $p = 0.044$  for peak current;  $p = 0.036$  for  $Q_{K1}$ ). Both the original mid-plateau  $I_{K1}$  values ( $p < 0.001$ ) and mid-plateau  $I_{K1}$  densities ( $p = 0.016$ ) showed significantly non-normal distribution, being right-skewed (towards larger values; skewnesses of 1.569 and 1.003, respectively), with CV values of 0.564 and 0.501, respectively. Mid-plateau  $I_{K1}$  densities, however, had only “medium” effect size of the non-normal distribution ( $\phi = 0.442$ ) compared to the “large” effect size ( $\phi = 0.738$ ) in case of the original mid-plateau  $I_{K1}$  values (Supplementary Table 3).

Bivariate distributions of  $C_m$  and  $I_{K1}$  peak as well as  $C_m$  and  $Q_{K1}$  data pairs were normal, whereas the bivariate distribution of  $C_m$  and mid-plateau  $I_{K1}$  was significantly different from normal ( $p < 0.001$ ). Correlations between  $C_m$  and  $I_{K1}$  peak ( $r = 0.785$ ,  $p < 0.001$ ), as well as  $C_m$  and  $Q_{K1}$  ( $r = 0.767$ ,  $p < 0.001$ ) data pairs were high; but for  $C_m$  and mid-plateau  $I_{K1}$ , no significant correlation was detected (see Fig. 3D–F and also Supplementary Table 6). Linear regression analysis between  $I_{K1}$  peak current and  $C_m$  yielded a slope of  $1.5 \pm 0.29$  pA/pF for the regression line, a value close to what has been reported as peak  $I_{K1}$  current density in canine ventricular cells<sup>14,16</sup>.

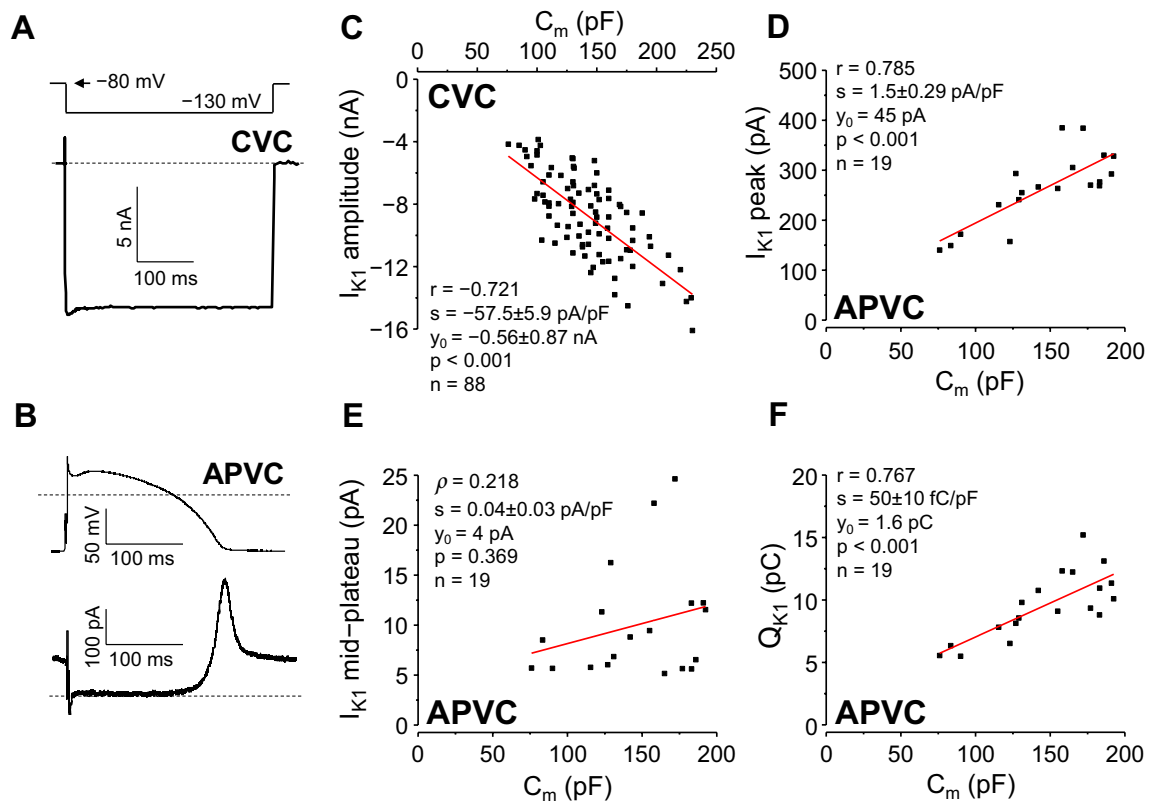


**Figure 3.** Correlation between  $C_m$  and  $I_{K1}$ . Left: representative inward  $I_{K1}$  current recorded at  $-130$  mV under CVC conditions (A) and outward  $I_{K1}$  record under APVC conditions (B). Command signals are shown above the current records, dashed lines indicate zero voltage and current levels. Right: correlations between  $C_m$  and  $I_{K1}$  amplitude, measured at the end of a 400 ms long hyperpolarization to  $-130$  mV under CVC conditions (C), peak amplitude of  $I_{K1}$  (D), mid-plateau amplitude of  $I_{K1}$  (E), and  $I_{K1}$  integral ( $Q_{K1}$ ; F) under APVC conditions. CVC experiments: 88 cells from 35 animals; APVC experiments: 19 cells from 11 animals.

### Rapid delayed rectifier $K^+$ current ( $I_{Kr}$ )

Under CVC conditions both the original  $I_{Kr}$  peak current (Fig. 4A) value and  $I_{Kr}$  peak current density distributions deviated significantly from normal distribution ( $p < 0.001$  and  $p = 0.013$ , respectively), being right-skewed (towards larger current values; skewness values of 0.904 and 0.548, respectively), with CVs being 0.458 (absolute) and 0.378 (normalized;  $p = 0.075$ ). After “normalizing” to  $C_m$ , the effect size of non-normal distribution changed from medium ( $\phi = 0.379$ ) to small ( $\phi = 0.221$ ). Similarly, bivariate distribution of  $C_m$  and  $I_{Kr}$  peak data pairs differed significantly from the normal distribution. Based on the results obtained in 120 myocytes the Spearman rank-correlation between  $I_{Kr}$  tail current amplitude and  $C_m$  was moderate ( $\rho = 0.628$ ,  $p < 0.001$ ; Fig. 4C). Linear regression analysis yielded a slope of  $0.49 \pm 0.05$  pA/pF.

Under APVC conditions  $I_{Kr}$  peaked during terminal repolarization (Fig. 4B). Contrary to CVC results, when  $I_{Kr}$  was investigated with APVC ( $n = 19$ ), all the measured parameters of the current, as well as their respective bivariate distributions with  $C_m$  followed normal distribution. The respective CV values for original and  $C_m$  “normalized” data were 0.359 and 0.266 for  $I_{Kr}$  peak; 0.632 and 0.58 for mid-plateau  $I_{Kr}$ ; whereas 0.397 and 0.289 for the charge carried by  $I_{Kr}$  ( $Q_{Kr}$ ). Although dividing the original current parameter values with  $C_m$  reduced CVs, these changes did not reach statistical significance.

High correlations for both  $I_{Kr}$  peak amplitude ( $r = 0.704$ ,  $p < 0.001$ ) and for  $Q_{Kr}$  ( $r = 0.709$ ,  $p < 0.001$ ) were obtained under these conditions (Fig. 4D,F). Similar to  $I_{K1}$ , the mid-plateau amplitude of  $I_{Kr}$  showed no significant correlation with  $C_m$  ( $r = 0.312$ ,  $p = 0.194$ , Fig. 4E). Linear regression analysis showed slope values of  $I_{Kr}$  current peak ( $0.49 \pm 0.12$  pA/pF) and  $Q_{Kr}$  ( $40 \pm 10$  fC/pF) similar to the current density and charge density values reported earlier for canine ventricular cells under APVC conditions<sup>16</sup>.

### Slow delayed rectifier $K^+$ current ( $I_{Ks}$ )

In case of  $I_{Ks}$  experiments (Fig. 5A), the membrane capacitance significantly deviated from normal distribution ( $p = 0.013$ ), with a medium effect size ( $\phi = 0.33$ ) when analyzing the results obtained from 79 myocytes under CVC conditions. The distribution was right-skewed (skewness = 0.765).

Both the original and  $C_m$  “normalized”  $I_{Ks}$  peak current value distributions deviated significantly from normal distribution ( $p < 0.001$  for both cases), being right-skewed (towards larger current values; skewness values of 1.448 and 0.886, respectively). Moreover, the absolute  $I_{Ks}$  peak values were also significantly leptokurtotic (with heavy tails; excess kurtosis = 2.544). CVs were 0.658 and 0.583, respectively. With “normalization” to  $C_m$ , the



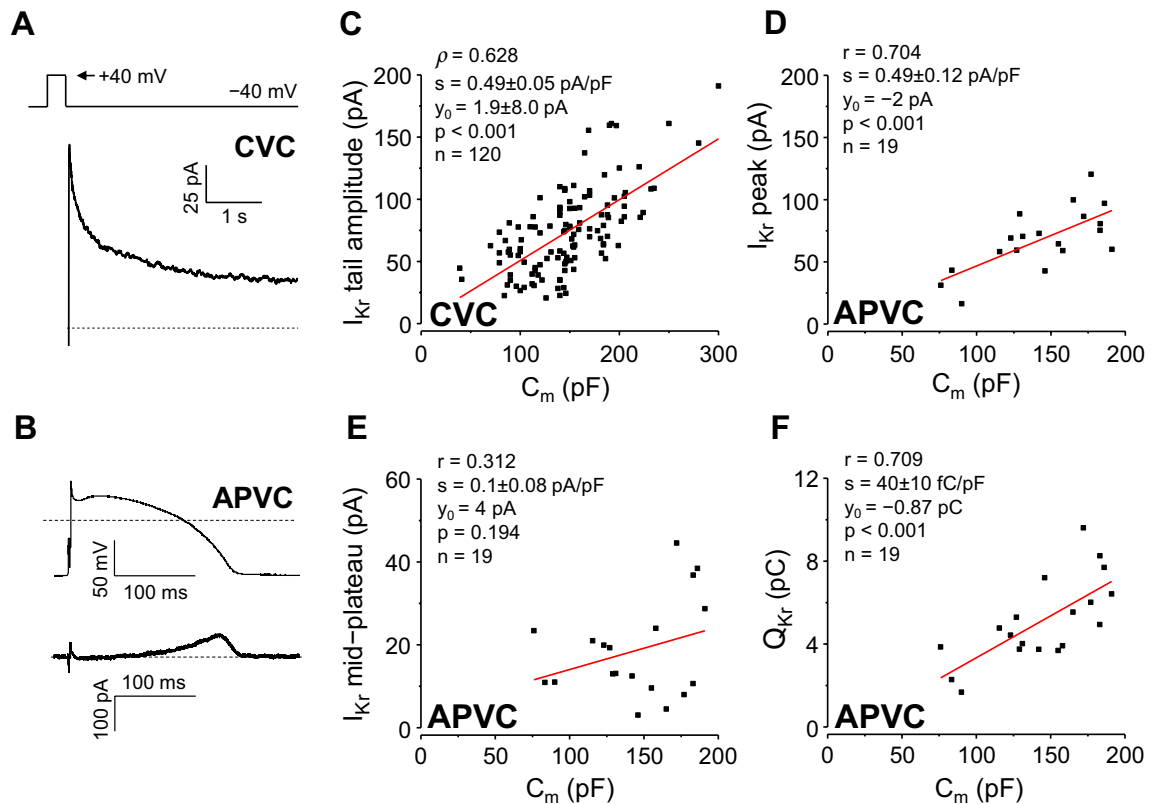


**Figure 4.** Correlation between  $C_m$  and  $I_{Kr}$ . Left: representative  $I_{Kr}$  tail current recorded at  $-40$  mV under CVC conditions (A) and an  $I_{Kr}$  current trace under APVC conditions (B). Command signals are shown above the current records, dashed lines indicate zero voltage and current levels. Right: correlations between  $C_m$  and  $I_{Kr}$  tail current amplitude under CVC conditions (C), peak  $I_{Kr}$  amplitude (D), mid-plateau  $I_{Kr}$  amplitude (E), and  $I_{Kr}$  integral ( $Q_{Kr}$ ; F) under APVC conditions. CVC experiments: 120 cells from 54 animals; APVC experiments: 19 cells from 10 animals.

effect size of the non-normal distribution was reduced from large ( $\phi = 0.592$ ) to medium ( $\phi = 0.359$ ). Similarly, bivariate distribution of  $C_m$  and  $I_{Ks}$  peak data pairs differed significantly from the bivariate normal distribution. Based on the results obtained the Spearman rank-correlation between  $I_{Ks}$  tail current amplitude and  $C_m$  was low ( $\rho = 0.223$ ,  $p = 0.048$ ; Fig. 5C), with a slope of  $1.04 \pm 0.27$  pA/pF.

Under APVC conditions,  $I_{Ks}$  rose slowly during the action potential plateau (Fig. 5B). Contrary to CVC results, when  $I_{Ks}$  was investigated with APVC ( $n = 18$ ), all the measured current parameters, as well as their respective bivariate distributions with  $C_m$  followed normal distribution. The respective CV values for original and  $C_m$  “normalized” data were 0.403 and 0.354 for  $I_{Ks}$  peak; 0.561 and 0.568 for mid-plateau  $I_{Ks}$ ; whereas 0.321 and 0.245 for the charge carried by  $I_{Ks}$  ( $Q_{Ks}$ ). Both  $C_m$  and  $I_{Ks}$  peak ( $r = 0.53$ ,  $p = 0.024$ ), as well as  $C_m$  and  $Q_{Ks}$  ( $r = 0.59$ ,  $p = 0.01$ ) correlated moderately, as demonstrated in Fig. 5D,F. No significant correlation was observed between mid-plateau  $I_{Ks}$  value and  $C_m$  (Fig. 5E). Linear regression analysis yielded slopes of  $0.16 \pm 0.08$  pA/pF for  $I_{Ks}$  peak, and  $12 \pm 4$  fC/pF for  $Q_{Ks}$ , respectively.

### Transient outward $K^+$ current ( $I_{to1}$ )

$I_{to1}$  was studied only under CVC conditions using myocytes ( $n = 108$ ) isolated from subepicardial (EPI), sub-endocardial (ENDO) and midmyocardial (MID) layers of the left ventricle. During our “regular” cell isolation method there is no physical separation of the transmural layers of the myocardium, therefore we are not able to distinguish between cells originating from the different myocardial layers. Because of the quite thin EPI and ENDO tissue layers, this method dominantly yields MID cells. However, when we cut off delicate layers of tissue from the epicardial and endocardial surface of the myocardium after the enzymatic digestion process (see in Methods and in<sup>17</sup>), myocytes of known origin (documented EPI, ENDO, MID cells;  $n = 30$ ,  $n = 15$ ,  $n = 18$ , respectively) can be obtained.

If all 108 cells were taken into consideration,  $C_m$  significantly deviated from normal distribution ( $p = 0.036$ ), being right-skewed (skewness = 0.61). However, the effect size of this deviation was small ( $\phi = 0.248$ ). In documented EPI, ENDO, MID as well as in presumably MID cells (all cells, except for EPI and ENDO cells),  $C_m$  followed normal distribution.

As shown in Fig. 6A, marked differences in  $I_{to1}$  amplitude were observed among the cells originating from different regions—in line with the known transmural heterogeneity of  $I_{to1}$  in canine ventricle<sup>18–20</sup>.

When all cells were analyzed together, both the original and the  $C_m$  “normalized”  $I_{to1}$  peak current distributions deviated significantly from normal distribution ( $p < 0.001$  for both cases), with similar “medium” effect sizes

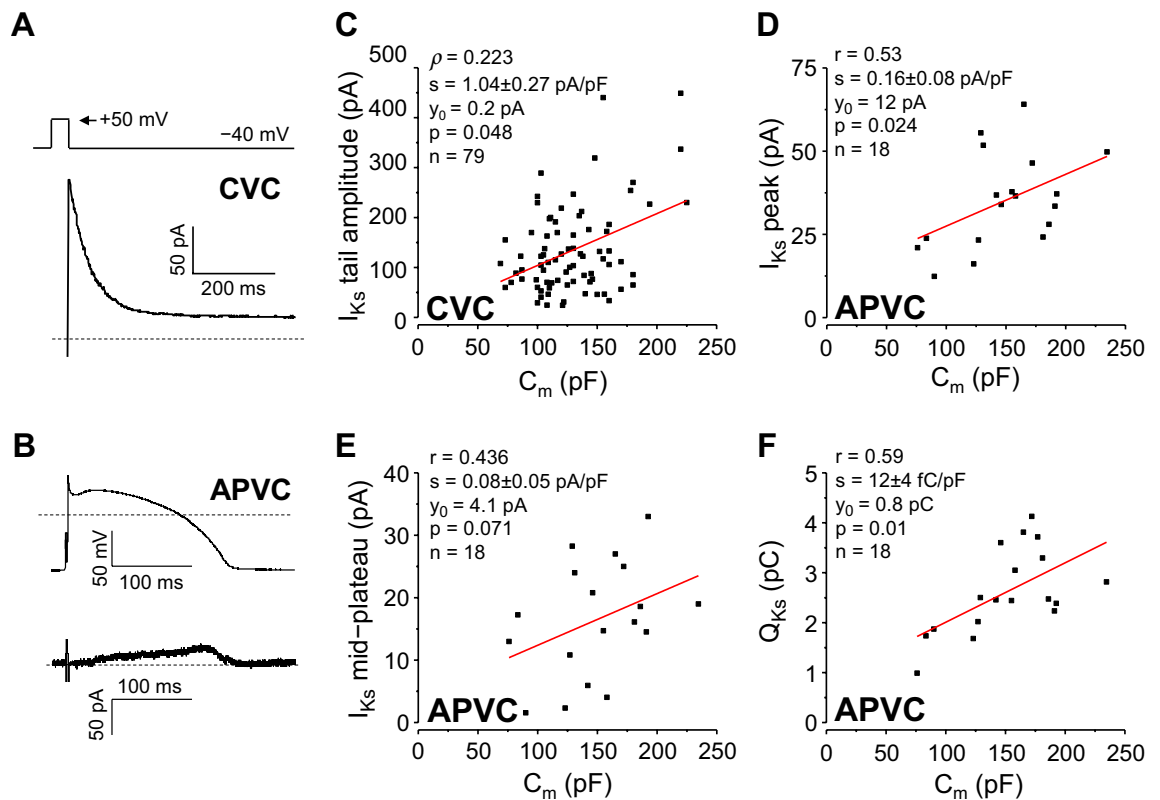


**Figure 5.** Correlation between  $C_m$  and  $I_{Ks}$ . Left: representative  $I_{Ks}$  tail current recorded at  $-40$  mV under CVC conditions (A) and  $I_{Ks}$  current under APVC conditions (B). Command signals are shown above the current records, dashed lines indicate zero voltage and current levels. Right: correlations between  $C_m$  and  $I_{Ks}$  tail current amplitude under CVC conditions (C), peak  $I_{Ks}$  amplitude (D), mid-plateau  $I_{Ks}$  amplitude (E), and  $I_{Ks}$  integral ( $Q_{Ks}$ ; F) under APVC conditions. CVC experiments: 79 cells from 27 animals; APVC experiments: 18 cells from 9 animals.

( $\phi = 0.334$  and  $\phi = 0.307$ ) and CVs (0.536 and 0.526), respectively. Both distributions were right-skewed (skewness values of 0.837 and 0.752, respectively). Similarly, bivariate distribution of  $C_m$  and  $I_{to1}$  peak data pairs differed significantly from the normal distribution ( $p < 0.001$ ). The Spearman rank-correlation between all  $I_{to1}$  peak current amplitudes and  $C_m$  was low, but statistically significant ( $\rho = 0.253$ ,  $p = 0.008$ , Fig. 6B; Supplementary Table 5).

*Documented* ENDO and MID cells shown normal peak current and  $C_m$  normalized peak current distributions, with CVs being 0.371 vs 0.28 (ENDO) and 0.377 vs 0.226 (MID) for absolute peak currents, and for normalized peak currents, respectively.

*Documented* EPI cells had normal peak current, but significantly non-normal  $C_m$  “normalized” peak current ( $p = 0.008$ ) distribution, with a large ( $\phi = 0.775$ ) effect size. CV of  $I_{to1}$  peak current density was significantly smaller (0.194) than in case of original peak current magnitudes (0.323). Visualizing the data revealed that the  $C_m$  normalized peak current distribution was non-normal because of an outlier cell having  $C_m = 80$  pF and a peak  $I_{to1}$  amplitude of 4399 pA, yielding a current density of 55 pA/pF. If we omitted this outlier from the Shapiro–Wilk test, no significant deviation from the normal distribution could be detected.

Even though there was a clear trend for a reduction in CV after normalizing to  $C_m$ , this effect was only significant in case of EPI cells ( $p = 0.012$ ).

Bivariate distributions of  $C_m$  and  $I_{to1}$  peak data pairs were normal in case of ENDO and MID myocytes, however in case of EPI cells, it significantly deviated from normal ( $p = 0.01$ ), because of the previously mentioned outlier cell. Data in cells of known origin showed strong and statistically significant correlations. Pearson’s correlation coefficients of 0.711 ( $p = 0.003$ ) and 0.825 ( $p < 0.001$ ) were obtained for *documented* ENDO and MID cells, respectively, whereas the Spearman’s correlation coefficient was 0.829 ( $p < 0.001$ ) in EPI myocytes. (Fig. 6C–E).

Myocytes of *presumably* MID origin (all cells except for the *documented* EPI and ENDO cells) showed significantly non-normal peak current ( $p = 0.007$ ,  $\phi = 0.345$ ), but normal peak current density ( $p = 0.081$ ) distributions, with a significantly reduced CV (from 0.386 to 0.266;  $p = 0.009$ ) after “normalization” to  $C_m$ . In these *presumably* MID myocytes, bivariate distribution of  $C_m$  and  $I_{to1}$  peak data pairs significantly deviated from normal ( $p = 0.003$ ). The correlation between  $C_m$  and  $I_{to1}$  peak was also high ( $\rho = 0.717$ ,  $p < 0.001$ ) in these cells (Fig. 6F). Comparing  $I_{to1}$  current densities obtained for the *documented* versus the *presumably* MID cells ( $22.6 \pm 3.9$  pA/pF vs  $16.8 \pm 2.0$  pA/pF, respectively) confirms the usual assumption that most of the myocytes of undefined origin were likely digested from the midmyocardial layer.

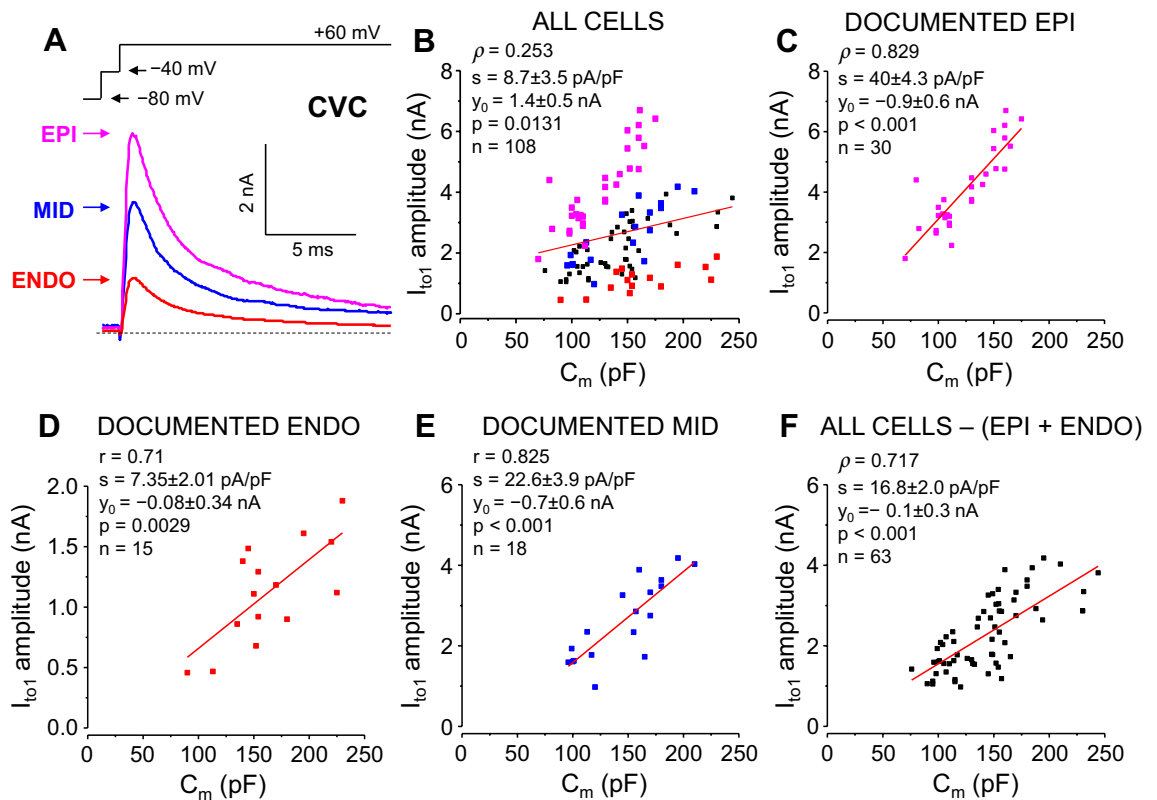


**Figure 6.** Correlation between  $C_m$  and  $I_{to1}$ . **(A)**: representative  $I_{to1}$  current records obtained at +60 mV under CVC conditions taken from a subepicardial (EPI; magenta), midmyocardial (MID; blue), and a subendocardial (ENDO, red) myocyte. The command voltage is shown above the current records, the dashed line indicates zero current level. **(B–F)**: Correlations between  $C_m$  and peak  $I_{to1}$  currents analyzed in various groups of myocytes. In panel **(B)**, all the 108 myocytes from 41 animals were included in the analysis, independent of their origin. In panels **(C, D and E)** cells with documented EPI (magenta), ENDO (red), or MID (blue) origin were analyzed, respectively, while in panel **F**, the presumably MID (non-EPI and non-ENDO cells; black) were considered. EPI experiments: 30 cells from 14 animals; ENDO experiments: 15 cells from 10 animals; MID experiments: 18 cells from 13 animals; presumably MID experiments: 63 cells from 36 animals.

## Discussion

This is the first study to systematically investigate a broad range of ion currents, obtained under two different voltage clamp conditions in canine ventricular myocytes to provide comprehensive statistical analyses of (1) the distribution of  $C_m$  and the ion current parameter values; (2) the relationship between  $C_m$  and the ion current parameters; and (3) the effect of “normalizing” the original membrane current parameters to  $C_m$ .

The distribution of  $C_m$  of all cells involved our study was significantly non-normal, being right-skewed, similar to the findings of Kula et al.<sup>5</sup>  $C_m$  values in case of any of the current groups did not deviate significantly from normal distribution, except in  $I_{Ks}$  measurements and when all cells were pooled together in  $I_{to1}$  measurements under CVC conditions. It is worth noting, however, that all normality tests get more and more sensitive to violations of normality as the sample size gets larger<sup>21</sup>, therefore we have found multiple deviations from normal distribution in our CVC experiments where sample sizes were at least  $n = 79$ .

Absolute peak current distributions obtained under CVC conditions were significantly non-normally distributed in case of  $I_{Ca,L}$ ,  $I_{Kr}$ ,  $I_{Ks}$ , and if all cells were pooled together in  $I_{to1}$  experiments (Supplementary Tables 1 and 2). Dividing peak current values with  $C_m$  (obtaining peak current densities) did not normalize the distributions, all of them remained significantly non-normal. However, effect sizes of the deviation from normal distribution, as well as CV values were smaller in the groups of peak current densities compared to the original peak currents. Reduction in CVs were statistically significant in cases of  $I_{Ca,L}$ ,  $I_{K1}$ , and  $I_{to1}$  (in the EPI and presumably MID groups). In their recent study, Kula et al.<sup>5</sup> also found significantly non-normal, right-skewed  $I_{K1}$  and  $I_{K(ACh)}$  current magnitude distributions with the Shapiro–Wilk test, and the calculated respective current densities were also significantly non-normally distributed. Ismaili and coworkers<sup>4</sup> studied distributions of  $I_{Ca,L}$  current peaks in various species, under different conditions. Most of their samples did not follow normal distribution and were seemingly right-skewed. When they divided  $I_{Ca,L}$  current peaks with  $C_m$  they had no consistent effect on CV, whereas in our study, the same operation significantly reduced CV in several cases. It is worth noting that in our studies, only 5 cells (less than 1% of all cells investigated) had  $C_m$  values less than 70 pF, whereas in the previously mentioned two studies<sup>4,5</sup>, a much larger proportion of the left ventricular cells had  $C_m$  values lower



than 70 pF, especially in rat samples. These more frequently occurring low  $C_m$  values might lead to a greater deviation from normal distribution.

Under APVC conditions, distributions of investigated current parameters did not differ significantly from the normal distribution in most cases, with the exceptions of mid-plateau  $I_{Na,late}$ ,  $Q_{Na,late}$ ,  $Q_{NCX}$  and mid-plateau  $I_{K1}$  (Supplementary Table 3). Dividing these current parameters with  $C_m$  “normalized” mid-plateau  $I_{Na,late}$ ,  $Q_{Na,late}$  and  $Q_{NCX}$  distributions, whereas distribution of the mid-plateau  $I_{K1}$  remained significantly non-normal, although the effect size of the deviation from non-normal distribution became much smaller ( $\phi = 0.738$  and  $\phi = 0.442$ , respectively; Supplementary Table 3). In general, CVs were non-significantly reduced after dividing with  $C_m$ , however, in the cases of peak  $I_{K1}$  and  $Q_{K1}$ , these reductions were statistically significant (Supplementary Table 3). In conclusion, we found dividing original data with  $C_m$  values generally useful, both by reducing the effect of the sometimes originally non-normal sample distributions (even rendering them normal in certain cases), as well as by reducing CVs of the samples.

Relationships between  $C_m$  and various ion current parameters were studied using *Pearson* and *Spearman* correlations and simple linear regression analysis under both APVC and CVC conditions. In case of many ion currents, including  $I_{Ca,L}$ ,  $I_{K1}$  and  $I_{Kr}$ , the correlation was usually high. Importantly, y intercepts of linear regression were close to zero indicating a true linear relationship between  $C_m$  and membrane current parameters ( $I_m$ ) for these ion currents. This is in line with the general assumption that ion current densities are constant, i.e. current amplitudes are linearly related to cell surface area. On the other hand, moderate correlation was obtained for  $I_{NCX}$  and low for  $I_{Na,late}$  and  $I_{Ks}$ .

Marked differences between individual ion currents of the same species regarding the correlation between  $C_m$  and  $I_m$  is not exceptional. Good correlation was found in rat myocytes in the case of  $I_{K1}$  but not for  $I_{to}^6$ —results identical to our observations in canine myocytes. Comparing the present results on canine  $I_{Ca,L}$  with those reported by Ismaili et al.<sup>4</sup> on human ventricular  $I_{Ca,L}$  (both obtained under CVC conditions) our correlation coefficient ( $r = -0.603$ ,  $r^2 = 0.364$ ) was higher than that reported by Ismaili et al. ( $r^2 = 0.28$ ). In that study the low correlation coefficient was attributed partially to inhomogeneous distribution of surface *versus* T-tubular localization of L-type  $Ca^{2+}$  channels<sup>22,23</sup>, which channel subpopulations might also be differently regulated<sup>24,25</sup>. This regional inhomogeneity at a cellular level may tremendously increase variability (mainly due to improper voltage control of T-tubular  $Ca^{2+}$  channels), however, these effects are likely similar in the cardiomyocytes of a given species.

Another possible reason for the low correlation between  $C_m$  and  $I_m$  might be a limited proportionality between the cell size and  $C_m$ <sup>4,6</sup>. Although the exact level of correlation between  $C_m$  and cell surface is not known, if there was any discrepancy between them, the relationship between  $C_m$  and  $I_m$  should have been affected similarly in the case of several ion currents. Furthermore, inaccurate  $C_m$  measurements<sup>26</sup> may also contribute to the limited proportionality between  $I_m$ ,  $C_m$ , and cell surface area. Again, however, even if there was any inaccuracy in measuring  $C_m$ , it likely had the same systemic effect on all cells. Although we cannot completely rule out that such an inaccuracy could have disproportionately affected certain groups of cells, therefore limiting the correlation between  $I_m$  and  $C_m$ .

Then, what might limit correlations between  $I_m$  and  $C_m$ ? Theoretically, there are at least three factors which might decrease the linear relationship between  $C_m$  and ion current amplitudes or integrals. These are: transmural and cell surface inhomogeneity of ion channel expression; small measured current values; and cell-to-cell variability of intracellular ion concentrations, especially  $[Ca^{2+}]_i$ .

Our results with  $I_{to1}$  represent a good example that regional inhomogeneity of ion channel expression is likely to be a limiting factor in significant correlations between  $I_m$  and  $C_m$ .  $I_{to1}$  is known to be abundantly expressed in the subepicardial layer, its expression is less pronounced in mid-myocardial cells, while the current is small in the subendocardial region of the canine heart<sup>17–20</sup>. Indeed, the correlation between  $I_{to1}$  and  $C_m$  was negligible ( $r = 0.21$ ) when all the cells were analyzed independently of their origin. In contrast, the correlation became much better when cells with documented origins were analyzed separately: correlation coefficients of  $\rho = 0.829$ ,  $r = 0.711$  and  $r = 0.825$  were obtained for subepicardial, subendocardial and midmyocardial cell populations, respectively. However, transmural inhomogeneity has been reported not only for  $I_{to1}$ , but also for  $I_{Na}$ ,  $I_{NCX}$  and  $I_{Ks}$ . More specifically, the density of  $I_{Na}$  is the highest in the mid-myocardial region and significantly lower in the subepicardial and subendocardial layers in dogs<sup>17,27,28</sup> and marked transmural inhomogeneity was observed in the case of  $I_{NCX}$  as well<sup>29,30</sup>. Regarding  $I_{Ks}$ , the density of the current is higher in the subepicardial than in the midmyocardial region<sup>17,31</sup>. Another type of regional inhomogeneity in the density of  $I_{Ks}$  was also observed. Expression of  $I_{Ks}$  was found to be more than double in the apical than in the basal region of the canine ventricular wall<sup>32</sup>. In contrast, no transmural inhomogeneity has been observed for  $I_{Ca,L}$ ,  $I_{Kr}$  or  $I_{K1}$  in canine ventricular myocardium<sup>17</sup>. Similarly, no apico-basal differences regarding the distribution of  $I_{K1}$  or  $I_{Kr}$  were demonstrated<sup>32</sup>.

Cell surface inhomogeneity of ion channel expression can also limit the correlation between certain currents and  $C_m$ . In differently sized cells, certain membrane compartments may represent different fractions of the total cell surface. For example, based on pure geometrical considerations, in short, wide cells, the relative membrane surface of intercalated discs is likely to be higher than in long, narrow ones. Therefore, the cell membrane of short, wide cells likely contains relatively more ion channels that are preferentially located in the intercalated discs (such as Nav1.5, Kir2.1 and Kir6.2<sup>33</sup>) than long, narrow cells. Finding out these discrepancies, however, are well beyond the scope of the present study.

An additional source of limited correlations between  $I_m$  and  $C_m$  may be the inherent inaccuracy of measurements. This error is expected to be larger when measuring currents with low amplitudes—a problem evident especially under APVC conditions. This issue is illustrated on Fig. 7, where the Pearson’s correlation coefficients obtained between  $C_m$  and certain ion current parameters are plotted as a function of their respective ion current densities. There were significant monotonic correlations between the Pearson’s correlation coefficients and their respective original current density values (Fig. 7A;  $\rho = 0.716$ ,  $p < 0.001$  for all currents;  $\rho = 0.833$ ,  $p = 0.015$  for

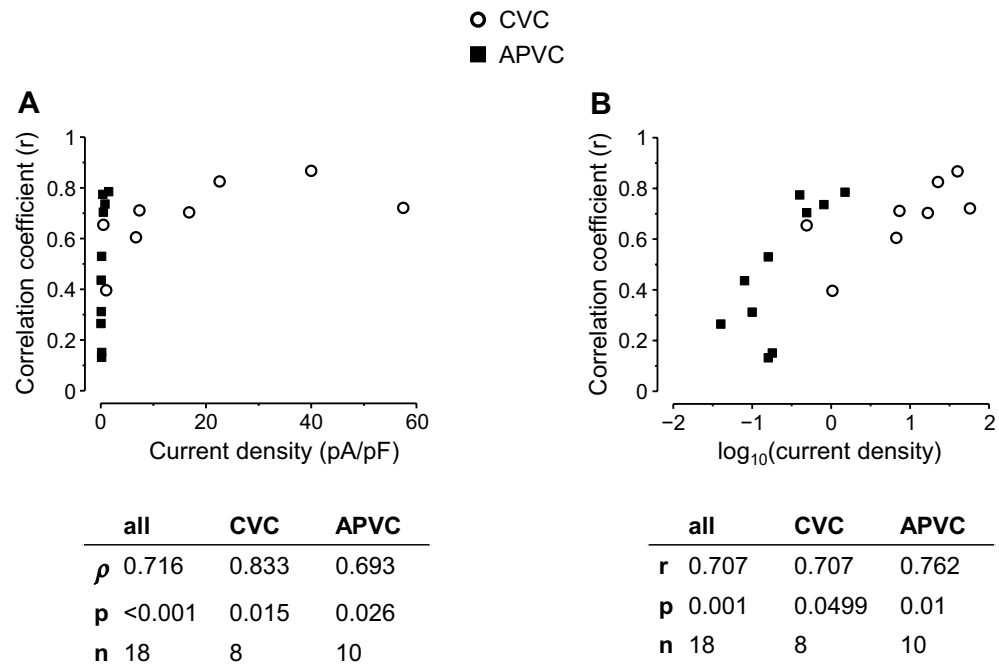


**Figure 7.** Relationship between Pearson's correlation coefficients and current densities in case of the studied currents and conditions. Open circles indicate data from conventional voltage clamp (CVC); whereas filled squares show data from action potential voltage clamp (APVC) experiments. **(A):** Pearson's correlation coefficients between  $C_m$  and ion current values are plotted against their respective ion current densities yielding significant monotonic (Spearman) correlations between them. **(B):** Pearson's correlation coefficients between  $C_m$  and ion current values plotted against the  $\log_{10}$  values of their respective ion current densities. There are significant linear relationships between these data pairs, suggesting a logarithmic relationship between data pairs of correlation coefficients of  $C_m$  versus ion current values and their respective ion current densities.

CVC;  $\rho = 0.693$ ,  $p = 0.026$  for APVC conditions), whereas after logarithmic transformation of the current density values, significant linear relationships could be seen (Fig. 7B;  $r = 0.707$ ,  $p = 0.001$  for all conditions;  $r = 0.707$ ,  $p = 0.0499$  for CVC;  $r = 0.762$ ,  $p = 0.01$  for APVC conditions). These correlations suggest a logarithmic association between the Pearson's correlation coefficients and their respective original current density values. This may explain the non-significant correlations between  $C_m$  and the mid-plateau amplitudes of  $I_{K1}$  and  $I_{Kr}$ , in sharp contrast with the significant and high correlations obtained for their peak amplitudes ( $r = 0.785$  and  $r = 0.704$ ;  $p < 0.001$  for both) or current integrals ( $r = 0.767$  and  $r = 0.709$ ;  $p < 0.001$  for both) under APVC conditions.

Inhomogeneity of intracellular  $Ca^{2+}$  concentration—a possible consequence of the variable  $Na^+$  and  $Ca^{2+}$  loads occurring during cell isolation—may also affect the correlation in the case of some strongly  $Ca^{2+}$ -dependent ion currents, such as  $I_{Ca,L}$  or  $I_{NCX}$ , but also  $I_{Na,late}$ <sup>34</sup> and  $I_{Ks}$ <sup>16</sup>. Furthermore, if the turnover of ion channels in the membrane may be fast enough, the time elapsed from cell isolation to the measurement may also influence the amplitude of an ion current<sup>35</sup>. Somewhat related to this, the relatively slow, but continuous reduction of current ion magnitude over time (ion current “run-down”) may also contribute to the limited correlations between  $I_m$  and  $C_m$ .

Since the experimental conditions were quite uniform in our APVC experiments, their results can be used for evaluation of effects of the above mentioned “burdens” on the correlation coefficients. This is summarized in Table 1, where all APVC experimental arrangements are included. According to these data, both regional inhomogeneity and low current amplitude are likely dominant reasons for limited proportionality between  $C_m$  and ion current amplitudes. Under APVC conditions it also must be noted that whenever the bivariate distribution of the investigated parameter and  $C_m$  was significantly (or marginally significantly) non-normal, no significant correlations were detected. These cases included the values of mid-plateau  $I_{Na,late}$ , mid-plateau  $I_{NCX}$ , mid-plateau  $I_{Kr}$  and mid-plateau  $I_{K1}$ . These infringements of normal bivariate distributions may arise from the above mentioned “burdens”, such as regional inhomogeneity of ion channel expression, small measured current values and variability of intracellular ion concentrations.

Our experiments performed under APVC conditions allowed the comparison of correlations found between  $C_m$  and  $I_m$  with those between  $C_m$  and current integrals. From this point of view, current integrals produced correlation coefficients at least as good as those obtained for peak current amplitudes. Furthermore, correlation coefficients obtained under APVC conditions were not lower than those estimated in CVC experiments, even though the number of cells analyzed in the APVC experiments was usually much lower than those used under CVC conditions.

Ion current	Parameter	Correlation coefficient	Non-normal distribution?	Regional differences	Low current amplitude
$I_{Ca,L}$	peak	-0.736	No		
	mid-plateau	-0.774	No		
	integral	-0.77	No		
$I_{Na,late}$	mid-plateau	-0.28	Yes	+	+
	integral	-0.475	No	+	+
$I_{NCX}$	mid-plateau	-0.145	Yes	+	+
	integral	-0.607	No	+	+
$I_{K1}$	peak	0.785	No		
	mid-plateau	0.218	Yes		+
	integral	0.767	No		
$I_{Kr}$	peak	0.704	No		
	mid-plateau	0.312	No ( $p=0.057$ )		+
	integral	0.709	No		
$I_{Ks}$	peak	0.53	No	+	+
	mid-plateau	0.436	No	+	+
	integral	0.59	No	+	+

**Table 1.** Burdens that might limit proportionality between ion current amplitudes and cell size under APVC conditions (+ : affected).

In summary, there is a clear tendency that dividing absolute values of ion current parameters with  $C_m$  reduces both the coefficient of variation, and the deviation from normal distribution, if there was any. In case of most currents, we found significant, moderate-to-high correlations between ion current amplitudes or integrals and  $C_m$ . However, the level of correlation between an ion current and  $C_m$  may be variable depending on the ion current studied, which must be considered when routinely evaluating ion current densities in cardiac cells.

## Methods

The study is reported in accordance with ARRIVE guidelines (<https://arriveguidelines.org>). For details regarding experimental animals, cell isolation procedure, and specific description of electrophysiology experiments, please refer to the *Supplementary Material*.

## Animals

Adult mongrel dogs of either sex were anesthetized with intramuscular injections of ketamine hydrochloride (10 mg/kg; Calypsol, Richter Gedeon, Hungary) and xylazine hydrochloride (1 mg/kg; Sedaxylan, Eurovet Animal Health BV, The Netherlands) according to a protocol approved by the local Animal Care Committee (license N°: 2/2020/DEMÁB, 9/2015/DEMÁB). All animal procedures conformed to the guidelines from Directive 2010/63/EU of the European Parliament.

## Electrophysiology

Cells were placed in a plexiglass chamber under an inverted microscope, allowing for continuous superfusion with a modified Tyrode solution by gravity flow at a rate of 1–2 ml/min. Under APVC conditions this solution contained (in mM): NaCl 121, KCl 4, CaCl<sub>2</sub> 1.3, MgCl<sub>2</sub> 1, HEPES 10, NaHCO<sub>3</sub> 25, glucose 10, while under CVC conditions it contained: NaCl, 144; KCl, 5; CaCl<sub>2</sub>, 2.5; MgCl<sub>2</sub>, 1.2; HEPES, 5; glucose, 10; both at pH = 7.35 and osmolality of 300 ± 3 mmol/kg. In all experiments, whole cell configuration of the patch clamp technique was applied<sup>36</sup>, where the bath temperature was set to 37 °C using a temperature controller (Cell MicroControls, Norfolk, VA, USA). Electrical signals were amplified and recorded (Axopatch 200B, MultiClamp 700A or 700B; Molecular Devices, Sunnyvale, CA, USA) under the control of a pClamp 6, 9 or 10 software (Molecular Devices) following analogue–digital conversion (Digidata 1200, 1322A or 1440A, Molecular Devices). Electrodes, having tip resistances of 2–3 MΩ when filled with pipette solution (pH = 7.3 and osmolality of 285 ± 3 mmol/kg), were fabricated from borosilicate glass. The series resistance was usually between 4 and 8 MΩ, and the experiment was discarded if it changed substantially during the measurement. Cell membrane capacitance ( $C_m$ ) was determined in each experiment by applying short (15 ms) hyperpolarizations from +10 to -10 mV.

## Conventional voltage clamp (APVC)

Experimental protocols applied under CVC conditions and the components of the bathing and pipette solutions are described in the *Supplementary Material*.

## Action potential voltage clamp (APVC)

APVC experiments were performed according to the methods described previously<sup>37–39</sup>. To avoid the consequences of cell-to-cell variations in AP morphology, the measurements were performed using a “canonic” AP as command signal, instead of the own AP of the cell. This canonic AP was chosen as a representative

midmyocardial canine AP characterized by average parameters. Application of uniform command APs made the comparison of the individual current traces easier. In these experiments the pipette solution contained (in mM): K-aspartate 120, KCl 30, MgATP 3, HEPES 10, Na<sub>2</sub>-phosphocreatine 3, EGTA 0.01, cAMP 0.002, KOH 10 at pH = 7.3 with an osmolarity of  $285 \pm 3$  mmol/kg. Ion currents were dissected pharmacologically by using their selective inhibitors. Accordingly,  $I_{Na,late}$  was dissected by 1  $\mu$ M GS-458967,  $I_{NCX}$  by 0.5  $\mu$ M ORM-10962,  $I_{Ca,L}$  by 1  $\mu$ M nisoldipine,  $I_{Kr}$  by 1  $\mu$ M E-4031,  $I_{Ks}$  by 0.5  $\mu$ M HMR-1556,  $I_{K1}$  by 50  $\mu$ M BaCl<sub>2</sub>, and  $I_{to1}$  by 100  $\mu$ M chromanol-293B applied in the presence of 0.5  $\mu$ M HMR-1556. Each drug-sensitive current was obtained by subtracting the post-drug trace from the pre-drug one. The cells were superfused for 3–5 min with the inhibitor before recording its effect, which record contained 20 consecutive current traces obtained at a cycle length of 0.7 s. These traces were averaged to reduce the noise and the trace-to-trace fluctuations. The dissected currents were evaluated by determining their maximum values (peak currents), their amplitudes measured at the half-duration of the command AP (mid-plateau current values), and finally the total charge carried by the current (current integrals, Q). During the analysis, the initial 10 ms after the AP upstroke was excluded to omit the capacitive transient.

### Statistics

We tested the normality of data distribution with the Shapiro–Wilk test, except for the distribution of  $C_m$ , where the D'Agostino–Pearson omnibus test was applied<sup>40,41</sup>. If there was a significant deviation from the normal distribution, the effect size of non-normality was also calculated as  $\phi$  values and were categorized as negligible ( $\phi < 0.1$ ), small ( $0.1 < \phi < 0.3$ ), medium ( $0.3 < \phi < 0.5$ ), or large effect ( $\phi > 0.5$ )<sup>41</sup>. For the description of data variance, we used the absolute value of the coefficient of variation (CV), defined as the standard deviation divided by the absolute value of the arithmetic mean. We used the *F* statistics proposed by Forkman<sup>42</sup> to test if dividing the original ion current parameter values with  $C_m$  (calculating ion current densities, or “normalizing”) caused any significant differences between CVs of original and “normalized” data.

For data pairs (eg.  $C_m$  and current magnitudes or  $C_m$  and current integrals), normality of the bivariate distribution was tested with the Shapiro–Wilk test for bivariate normality. If the bivariate distribution of data pairs did not differ significantly from the bivariate normal distribution, correlation between the two variables is described with the *Pearson's correlation coefficient* (*r*) for linear association. In case of data pairs with significantly non-normal bivariate distribution, *Spearman's correlation coefficient* ( $\rho$ , “rho”) for monotonic association is reported. The significance of correlation (*p*) was also calculated. To provide a comprehensive overview of correlation analysis, parameters for both the *Pearson's* and *Spearman's* correlations are reported for all investigated ion current parameters in Supplementary Tables 4, 5 and 6. For further information on correlation analysis and the bivariate normal distribution, see the *Supplementary Material*. Significant correlations were categorized according to the calculated coefficient: high ( $0.9 \geq |r| > 0.7$  or  $0.9 \geq |\rho| > 0.7$ ), moderate ( $0.7 \geq |r| > 0.5$  or  $0.7 \geq |\rho| > 0.5$ ), low ( $0.5 \geq |r| > 0.3$ ,  $0.5 \geq |\rho| > 0.3$ ) or negligible ( $0.3 > |r|$  or  $0.3 > |\rho|$ )<sup>43</sup>.

Besides correlation analysis, we also performed simple linear regression with  $C_m$  as the predictor variable, and the different current parameters (peak amplitude, mid-plateau value, current integral) being response variables. Figures show the slope of the fitted line (*s*) and the *y* intercept ( $y_0$ ), expressed as mean  $\pm$  SEM values, whereas (*n*) denotes the number of myocytes studied.

For statistical analyses, we mainly used Jeffreys's Amazing Statistics Program (JASP; version 0.16.1, Amsterdam, The Netherlands). We also used Origin 2015 (OriginLab Corporation, Northampton, MA, USA) for simple linear regression, and the Statistics Kingdom website<sup>41</sup> for calculating the D'Agostino–Pearson omnibus test, and the effect size of non-normality ( $\phi$ ). Results were considered statistically significant in case of  $p < 0.05$ ; in the summary tables, all  $p < 0.1$  values are reported.

### Data availability

Data underlying this article are available in the Open Science Framework, at <https://doi.org/10.17605/OSF.IO/5X428>.

Received: 21 February 2024; Accepted: 9 May 2024

Published online: 16 May 2024

### References

1. Fricke, H. The electric capacity of suspensions with special reference to blood. *J. Gen. Physiol.* **9**(2), 137–152 (1925).
2. Cole, K. S. *Membranes, Ions and Impulses: A Chapter of Classical Biophysics* (University of California Press, 1972).
3. Gentet, L. J., Stuart, G. J. & Clements, J. D. Direct measurement of specific membrane capacitance in neurons. *Biophys. J.* **79**(1), 314–320 (2000).
4. Ismaili, D., Geelhoed, B. & Christ, T. Ca(2+) currents in cardiomyocytes: How to improve interpretation of patch clamp data?. *Prog. Biophys. Mol. Biol.* **157**, 33–39 (2020).
5. Kula, R., Bébarová, M., Matejovič, P., Šimurda, J. & Pásek, M. Distribution of data in cellular electrophysiology: Is it always normal?. *Prog. Biophys. Mol. Biol.* **157**, 11–17 (2020).
6. Kula, R., Bébarová, M., Matejovič, P., Šimurda, J. & Pásek, M. Current density as routine parameter for description of ionic membrane current: Is it always the best option?. *Prog. Biophys. Mol. Biol.* **157**, 24–32 (2020).
7. Muszkiewicz, A. *et al.* From ionic to cellular variability in human atrial myocytes: An integrative computational and experimental study, *American journal of physiology. Heart Circ. Physiol.* **314**(5), H895–H916 (2018).
8. Gemmel, P., Burrage, K., Rodriguez, B. & Quinn, T. A. Rabbit-specific computational modelling of ventricular cell electrophysiology: Using populations of models to explore variability in the response to ischemia. *Prog. Biophys. Mol. Biol.* **121**(2), 169–184 (2016).
9. Ballouz, S. *et al.* Co-expression of calcium and hERG potassium channels reduces the incidence of proarrhythmic events. *Cardiovasc. Res.* **117**(10), 2216–2227 (2021).

10. Lachaud, Q. *et al.* Electrophysiological heterogeneity in large populations of rabbit ventricular cardiomyocytes. *Cardiovasc. Res.* **118**(15), 3112–3125 (2022).
11. Muszkiewicz, A. *et al.* Variability in cardiac electrophysiology: Using experimentally-calibrated populations of models to move beyond the single virtual physiological human paradigm. *Progr. Biophys. Mol. Boil.* **120**(1–3), 115–127 (2016).
12. Britton, O. J. *et al.* Experimentally calibrated population of models predicts and explains intersubject variability in cardiac cellular electrophysiology. *Proc. Natl. Acad. Sci. USA* **110**(23), E2098–E2105 (2013).
13. Jameson, M. B., Rios-Perez, E. B., Liu, F., Eichel, C. A. & Robertson, G. A. Pairwise biosynthesis of ion channels stabilizes excitability and mitigates arrhythmias. *Proc. Natl. Acad. Sci. USA* **120**(42), e2305295120 (2023).
14. Jost, N. *et al.* Contribution of I Kr and I K1 to ventricular repolarization in canine and human myocytes: Is there any influence of action potential duration?. *Basic Res. Cardiol.* **104**(1), 33–41 (2009).
15. Jost, N. *et al.* Ionic mechanisms limiting cardiac repolarization reserve in humans compared to dogs. *J. Physiol.* **591**(17), 4189–4206 (2013).
16. Horvath, B. *et al.* Ion current profiles in canine ventricular myocytes obtained by the “onion peeling” technique. *J. Mole. Cell. Cardiol.* **158**, 153–162 (2021).
17. Szabo, G. *et al.* Asymmetrical distribution of ion channels in canine and human left-ventricular wall: Epicardium versus midmyocardium. *Pflugers Archiv: Eur. J. Physiol.* **450**(5), 307–316 (2005).
18. Antzelevitch, C. *et al.* Heterogeneity within the ventricular wall. Electrophysiology and pharmacology of epicardial, endocardial, and M cells. *Circ. Res.* **69**(6), 1427–1449 (1991).
19. Liu, D. W., Gintant, G. A. & Antzelevitch, C. Ionic bases for electrophysiological distinctions among epicardial, midmyocardial, and endocardial myocytes from the free wall of the canine left ventricle. *Circ. Res.* **72**(3), 671–687 (1993).
20. Litovsky, S. H. & Antzelevitch, C. Transient outward current prominent in canine ventricular epicardium but not endocardium. *Circ. Res.* **62**(1), 116–126 (1988).
21. N.M. Razali, Y.B. Wah, Power comparisons of Shapiro-Wilk, Kolmogorov-Smirnov, Lilliefors and Anderson-Darling tests, (2011).
22. Glukhov, A. V. *et al.* Direct evidence for microdomain-specific localization and remodeling of functional L-type calcium channels in rat and human atrial myocytes. *Circulation* **132**(25), 2372–2384 (2015).
23. Sanchez-Alonso, J. L. *et al.* Microdomain-specific modulation of L-type calcium channels leads to triggered ventricular arrhythmia in heart failure. *Circ. Res.* **119**(8), 944–955 (2016).
24. Balijepalli, R. C., Foell, J. D., Hall, D. D., Hell, J. W. & Kamp, T. J. Localization of cardiac L-type Ca(2+) channels to a caveolar macromolecular signaling complex is required for beta(2)-adrenergic regulation. *Proc. Natl. Acad. Sci. USA* **103**(19), 7500–7505 (2006).
25. Best, J. M. & Kamp, T. J. Different subcellular populations of L-type Ca<sup>2+</sup> channels exhibit unique regulation and functional roles in cardiomyocytes. *J. Mol. Cell. Cardiol.* **52**(2), 376–387 (2012).
26. Platzer, D. & Zorn-Pauly, K. Accuracy considerations for capacitance estimation by voltage steps in cardiomyocytes. *Progr. Biophys. Mole. Biol.* **157**, 3–10 (2020).
27. Zygmunt, A. C., Eddlestone, G. T., Thomas, G. P., Nesterenko, V. V. & Antzelevitch, C. Larger late sodium conductance in M cells contributes to electrical heterogeneity in canine ventricle, *American journal of physiology. Heart Circ. Physiol.* **281**(2), H689–H697 (2001).
28. Atzelevitch, C. & Belardinelli, L. The role of sodium channel current in modulating transmural dispersion of repolarization and arrhythmogenesis. *J. Cardiovasc. Electrophysiol.* **17**(Suppl 1), S79–S85 (2006).
29. Zygmunt, A. C., Goodrow, R. J. & Antzelevitch, C. I(NaCa) contributes to electrical heterogeneity within the canine ventricle, *American journal of physiology. Heart Circ. Physiol.* **278**(5), H1671–H1678 (2000).
30. Xiong, W., Tian, Y., DiSilvestre, D. & Tomaselli, G. F. Transmural heterogeneity of Na<sup>+</sup>-Ca<sup>2+</sup> exchange: Evidence for differential expression in normal and failing hearts. *Circ. Res.* **97**(3), 207–209 (2005).
31. Liu, D. W. & Antzelevitch, C. Characteristics of the delayed rectifier current (IKr and IKs) in canine ventricular epicardial, midmyocardial, and endocardial myocytes. A weaker IKs contributes to the longer action potential of the M cell. *Circ. Res.* **76**(3), 351–365 (1995).
32. Szentadrassy, N. *et al.* Apico-basal inhomogeneity in distribution of ion channels in canine and human ventricular myocardium. *Cardiovasc. Res.* **65**(4), 851–860 (2005).
33. Vermij, S. H., Abriel, H. & van Veen, T. A. B. Refining the molecular organization of the cardiac intercalated disc. *Cardiovasc. Res.* **113**(3), 259–275 (2017).
34. Kiss, D. *et al.* Late Na<sup>+</sup> current I<sub>s</sub> [Ca<sup>2+</sup>]<sub>i</sub>-dependent in canine ventricular myocytes. *Pharmaceuticals* **14**(11), 1142. <https://doi.org/10.3390/ph14111142> (2021).
35. Chien, A. J. *et al.* Roles of a membrane-localized beta subunit in the formation and targeting of functional L-type Ca<sup>2+</sup> channels. *J. Boil. Chem.* **270**(50), 30036–30044 (1995).
36. Hamill, O. P., Marty, A., Neher, E., Sakmann, B. & Sigworth, F. J. Improved patch-clamp techniques for high-resolution current recording from cells and cell-free membrane patches. *Pflugers Archiv: Eur. J. Physiol.* **391**(2), 85–100 (1981).
37. Banyasz, T. *et al.* Action potential clamp fingerprints of K<sup>+</sup> currents in canine cardiomyocytes: Their role in ventricular repolarization. *Acta Physiologica* **190**(3), 189–198 (2007).
38. Bányász, T. *et al.* Endocardial versus epicardial differences in L-type calcium current in canine ventricular myocytes studied by action potential voltage clamp. *Cardiovasc. Res.* **58**(1), 66–75 (2003).
39. Horvath, B. *et al.* Late sodium current in human, canine and guinea pig ventricular myocardium. *J. Mol. Cell. Cardiol.* **139**, 14–23 (2020).
40. D’Agostino, R. B. & Belanger, A. A suggestion for using powerful and informative tests of normality. *Am. Statistician* **44**(4), 316–321 (1990).
41. D’Agostino-Pearson Test Calculator, 2017. <https://www.statskingdom.com/dagostino-pearson-test-calculator.html>. (Accessed 20 March 2022).
42. Forkman, J. Estimator and tests for common coefficients of variation in normal distributions. *Commun. Statist. - Theory Methods* **38**(2), 233–251 (2009).
43. D.E. Hinkle, W. Wiersma, S.G. Jurs, Applied Statistics for the Behavioral Sciences, Houghton Mifflin2003.

## Acknowledgements

This work was funded by the National Research, Development and Innovation Office (NKFIH-K138090 to PPN, NKFIH-K142764 to NSz, NKFIH-K147301 to TB and NKFIH-FK128116 to BH) and by the Hungarian Academy of Sciences (János Bolyai Research Scholarship to BH). Further support was obtained from the National Research, Development and Innovation Fund of Hungary, financed under the 2020-4.1.1-TKP2020 funding scheme (TKP2020-NKA-04). ZsK CsD and ZB obtained further support from the New National Excellence Program (ÚNKP-23-3-II-DE-109, ÚNKP-23-4-I-DE-64 and ÚNKP-22-2-I-DE-389, respectively).



### Author contributions

Conceptualization: B.H., P.P.N.; Experimental design: B.H., N.S., J.M., T.B., P.P.N.; Data acquisition: B.H., Z.K., C.D., J.O., N.S., T.B., J.M.; Data analysis: B.H., Z.B.; Visualization: B.H., Z.B., N.S.; Data interpretation: B.H., T.B., P.P.N.; writing—original draft preparation: B.H., C.D., Z.K.; Z.B., O.J.; writing—review and editing: J.M., T.B., P.P.N.; supervision: B.H., N.S., P.P.N.; funding acquisition: B.H., N.S., P.P.N. All persons designated as authors qualify for authorship, and all those who qualify for authorship are listed. All authors have read and approved to the submitted version of the manuscript and agreed to be accountable for all aspects of the work in ensuring that questions related to the accuracy or integrity of any part of the work are appropriately investigated and resolved.

### Funding

Open access funding provided by University of Debrecen.

### Competing interests

The authors declare no competing interests.

### Additional information

**Supplementary Information** The online version contains supplementary material available at <https://doi.org/10.1038/s41598-024-61736-6>.

**Correspondence** and requests for materials should be addressed to B.H.

**Reprints and permissions information** is available at [www.nature.com/reprints](http://www.nature.com/reprints).

**Publisher's note** Springer Nature remains neutral with regard to jurisdictional claims in published maps and institutional affiliations.



**Open Access** This article is licensed under a Creative Commons Attribution 4.0 International License, which permits use, sharing, adaptation, distribution and reproduction in any medium or format, as long as you give appropriate credit to the original author(s) and the source, provide a link to the Creative Commons licence, and indicate if changes were made. The images or other third party material in this article are included in the article's Creative Commons licence, unless indicated otherwise in a credit line to the material. If material is not included in the article's Creative Commons licence and your intended use is not permitted by statutory regulation or exceeds the permitted use, you will need to obtain permission directly from the copyright holder. To view a copy of this licence, visit <http://creativecommons.org/licenses/by/4.0/>.

© The Author(s) 2024